RESSALVA

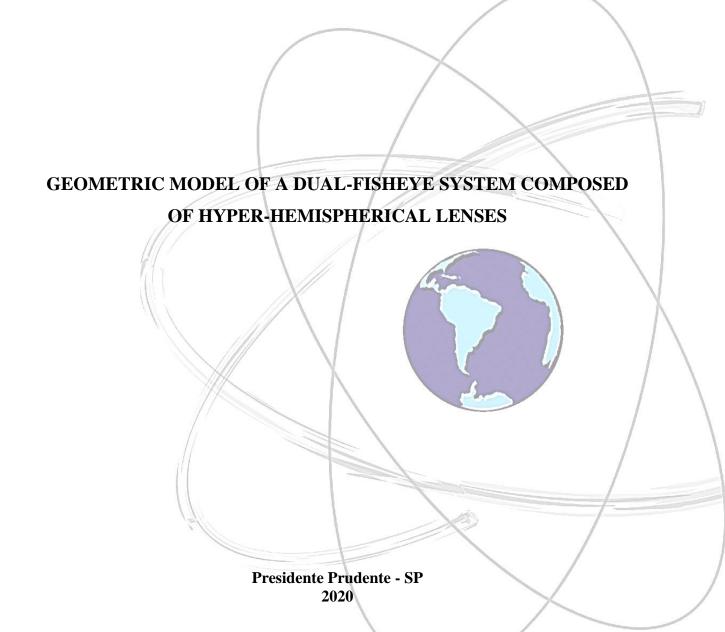
Atendendo solicitação do(a) autor(a), o texto completo desta dissertação será disponibilizado somente a partir de 03/03/2022.



UNESP – UNIVERSIDADE ESTADUAL PAULISTA

CAMPUS DE PRESIDENTE PRUDENTE FACULDADE DE CIÊNCIAS E TECNOLOGIA PÓS GRADUAÇÃO EM CIÊNCIAS CARTOGRÁFICAS

LETÍCIA FERRARI CASTANHEIRO



LETÍCIA FERRARI CASTANHEIRO

GEOMETRIC MODEL OF A DUAL-FISHEYE SYSTEM COMPOSED OF HYPER-HEMISPHERICAL LENSES

Master's thesis presented to "Programa de Pós-Graduação em Ciências Cartográficas" at School of Sciences and Technology of São Paulo State University – FCT/UNESP to obtain the degree of master of Cartographic Sciences.

Supervisor: Prof. Dr. Antonio Maria Garcia

Tommaselli

Co-supervisor: Prof. Dr. Adilson Berveglieri

Castanheiro, Letícia Ferrari
C346g
Geometric model of a dua

Geometric model of a dual-fisheye system composed of hyper-hemispherical lenses / Letícia Ferrari Castanheiro. -- Presidente Prudente, 2020

86 f.

Dissertação (mestrado) - Universidade Estadual Paulista (Unesp), Faculdade de Ciências e Tecnologia, Presidente Prudente Orientador: Antonio Maria Garcia Tommaselli

Coorientador: Adilson Berveglieri

1. hyper hemispherical lens. 2. fisheye model. 3. omnidirectional system. 4. multi-camera calibration. 5. stability constraints. I. Título.

Sistema de geração automática de fichas catalográficas da Unesp. Biblioteca da Faculdade de Ciências e Tecnologia, Presidente Prudente. Dados fornecidos pelo autor(a).

Essa ficha não pode ser modificada.



UNIVERSIDADE ESTADUAL PAULISTA

Câmpus de Presidente Prudente

CERTIFICADO DE APROVAÇÃO

TÍTULO DA DISSERTAÇÃO: Geometric model of a dual-fisheye system composed of hyper-hemispherical lenses

AUTORA: LETÍCIA FERRARI CASTANHEIRO

ORIENTADOR: ANTONIO MARIA GARCIA TOMMASELLI

COORIENTADOR: ADILSON BERVEGLIERI

Aprovada como parte das exigências para obtenção do Título de Mestra em CIÊNCIAS CARTOGRÁFICAS, área: Aquisição, Análise e Representação de Informações Espaciais pela Comissão Examinadora:

Prof. Dr. ANTONIO MARIA GARCIA TOMMASELLI

Departamento de Cartografia / Faculdade de Ciencias e Tecnologia de Presidente Prudente

Prof. Dr. MARIO LUIZ LOPES REISS

Departamento de Geodésia / Universidade Federal de Rio Grande do Sul

Prof. Dr. MAURICIO GALO

Departamento de Cartografia / Faculdade de Ciencias e Tecnologia de Presidente Prudente

Presidente Prudente, 03 de março de 2020

To those who gave me support and will not read it: My lovely family, Lislene, Pedro e André, examples of honesty and dedication. My friend Melina for her advices, patience and for being the best roomie during my academic journey.

ACKNOWLEDGMENTS

This study was funded in part by the Coordenação de Aperfeiçoamento de Pessoal de Nível Superior – Brasil (CAPES) – Finance Code 001 (Grants: 1774590, 88882.433941/2019-01 and 88881.310314/2018-01).

This work was also supported by Fundação de Amparo à Pesquisa do Estado de São Paulo (FAPESP - Grant: 2013/50426-4) and Academy of Finland (Grant: 273806), which jointly funded the international project Unmanned Airborne Vehicle -based 4D Remote Sensing for mapping rain forest biodiversity and its change in Brazil (UAV_4D_Bio).

I would like to thank the UNESP (São Paulo State University) – School of Technology and Sciences and PPGCC (Postgraduate program in Cartographic Sciences) for all support and infrastructure to develop this research. I would like also to thank AGT-Bravium-Fundunesp for all support offered to develop field campaigns.

I am thankful to my supervisor, Prof. Dr. Antonio M. G. Tommaselli, and co-supervisor, Prof. Dr. Adilson Berveglieri, for their guidance and their support in this research.

I would like also to thank Photogrammetry group of FCT-UNESP for exchanges of experience and for helping to improve the calibration field.

I am thankful to my friends from PPGCC for their support and collaboration in the development of this work. In particular, I would like to thank my dear friend Mariana B. Campos, who contributed in the development of this work providing the calibration data, helping in the processing and giving interesting discussions. Also, I would like to thank José Marco Junior for his work implementing the fisheye models and for technical support.

"We must have perseverance and above all confidence in ourselves." Marie Curie "You only learn from experience, so as much as someone can tell you things, you have to go out there and make your own mistakes in order to learn." Emma Watson

RESUMO

A combinação de duas lentes com FOV hiper-hemisférico em posição opostas pode gerar um sistema omnidirecional (FOV 360°) leve, compacto e de baixo custo, como Ricoh Theta S e GoPro Fusion. Entretanto, apenas algumas técnicas e modelos matemáticos para a calibração um sistema com duas lentes hiper-hemisféricas são apresentadas na literatura. Nesta pesquisa, é avaliado e definido um modelo geométrico para calibração de sistemas omnidirecionais compostos por duas lentes hiper-hemisféricas e apresenta-se algumas aplicações com esse tipo de sistema. A calibração das câmaras foi realizada no programa CMC (calibração de múltiplas câmeras) utilizando imagens obtidas a partir de vídeos feitos com a câmara Ricoh Theta S no campo de calibração 360°. A câmara Ricoh Theta S é composto por duas lentes hiperhemisféricas fisheye que cobrem 190° cada uma. Com o objetivo de avaliar as melhorias na utilização de pontos em comum entre as imagens, dois conjuntos de dados de pontos foram considerados: (1) apenas pontos no campo hemisférico, e (2) pontos em todo o campo de imagem (isto é, adicionar pontos no campo de imagem hiper-hemisférica). Primeiramente, os modelos ângulo equisólido, equidistante, estereográfico e ortogonal combinados com o modelo de distorção Conrady-Brown foram testados para a calibração de um sensor da câmara Ricoh Theta S. Os modelos de ângulo-equisólido e estereográfico apresentaram resultados melhores do que os outros modelos. Portanto, esses dois modelos de projeção foram utilizados em uma calibração simultânea da câmera (ou seja, ambos os sensores Ricoh Theta S foram considerados em um mesmo procedimento). POIs (parâmetros de orientação interior) e POEs (parâmetros de orientação exterior) de ambos os sensores, e POR (parâmetros de orientação relativa) foram estimados em um ajustamento de blocos com injunção de estabilidade dos ROPs. Os modelos ângulo-equisólido e estereográfico apresentaram bons resultados com o uso dos pontos na área hiper-hemisférica da imagem para a estimação dos POIs, POEs e PORs. No entanto, o ajustamento baseado no modelo ângulo-equisólido com injunção de estabilidade apresentou os melhores resultados. Neste trabalho, também é apresentado duas aplicações com sistemas omnidirecionais: mapeamento 3D de uma área urbana usando um sistema de mapeamento móvel terrestre, composto pela câmara Ricoh Theta S, e a geração da nuvem 3D de uma área agrícola com a câmara GoPro Fusion, que também é composta por duas lentes hiperhemisféricas. Ambos experimentos apresentaram o potencial do uso de sistemas omnidirecionais na geração de nuvem de pontos fotogramétrica e extração de atributos importantes para cada aplicação.

Palavras-chaves: lente hiper-hemisférica; modelos de projeção *fisheye*; sistema omnidirecional; sistema polidióptrico; calibração de múltiplas câmaras; injunção de estabilidade; mapeamento 3D.

ABSTRACT

The arrangement of two hyper-hemispherical fisheye lenses in opposite position can design a light weight, small and low-cost omnidirectional system (360° FOV), e.g. Ricoh Theta S and GoPro Fusion. However, only a few techniques are presented in the literature to calibrate a dual-fisheye system. In this research, a geometric model for dual-fisheye system calibration was evaluated, and some applications with this type of system are presented. The calibrating bundle adjustment was performed in CMC (calibration of multiple cameras) software by using the Ricoh Theta video frames of the 360° calibration field. The Ricoh Theta S system is composed of two hyper-hemispherical fisheye lenses with 190° FOV each one. In order to evaluate the improvement in applying points in the hyper-hemispherical image field, two data set of points were considered: (1) observations that are only in the hemispherical field, and (2) points in all image field, i.e. adding points in the hyper-hemispherical image field. First, one sensor of the Ricoh Theta S system was calibrated in a bundle adjustment based on the equidistant, equisolid-angle, stereographic and orthogonal models combined with Conrady-Brown distortion model. Results showed that the equisolid-angle and stereographic models can provide better solutions than those of the others projection models. Therefore, these two projection models were implemented in a simultaneous camera calibration, in which the both Ricoh Theta sensors were considered in a same procedure. IOPs (interior orientation parameters) and EOPs (exterior orientation parameters) of both sensors, and a set of ROPs (relative orientation parameters) were estimated in a bundle adjustment based on stability constraints of ROPs. Both equisolid-angle and stereographic models presented good performances; meanwhile, the equisolid-angle model showed more stable results than stereographic model when adding observation in the hyper-hemispherical image field. In this research, two applications applying dual-fisheye cameras are also investigated: 3D city mapping using a PMTS (portable mobile terrestrial system) that is composed of Ricoh Theta S dual-camera, and 3D crop modelling using GoPro Fusion dual-camera. Both experimental assessments presented the potential advantage of using the omnidirectional system to generate a 3D point cloud, in which can extract important attributes for each application.

Keywords: hyper-hemispherical lens, fisheye projection model, omnidirectional system, polydioptric system, multi-camera calibration, stability constraints, 3D mapping.

LIST OF FIGURES

Figure 1 - Collinearity condition
Figure 2 – Fisheye lenses: (a) projection geometry and (b) an example of a fisheye image23
Figure 3 – Projection geometry of (a) equidistant, (b) equisolid-angle, (c) stereographic, and (d) orthogonal models.
Figure 4 - Photogrammetric and image systems of the (a) perspective and equidistant projections, and (b) orthogonal, stereographic and equisolid-angle projections25
Figure 5 - 360° camera calibration field: (a) a fisheye image, in which the local reference system (right-handed) is depicted, and an example of (b) ArUco target and (c) coded target (CT) from Agisoft Metashape
Figure 6 – ArUco detection with a fisheye image, in which the origin of the local reference system can be seen
Figure 7 – Ricoh Theta S (a) dual-camera, (b) top view, (c) set of lenses and the path of the light rays to sensors, (d) video frames from sensor 1 (S1) and sensor 2 (S2) and (e) a 360° equirectangular image
Figure 8 - 360° circular target structure: (a) Ricoh Theta S camera in the center of the circular target, (b) dual-fisheye image from sensor 1 (S1) and sensor 2 (S2) and (c) the gradation strip on the circular target.
Figure 9 – Geometry of a point P in the object space, projected in the fisheye image (p) and then reprojected on the sphere (Ps)
Figure 10 – Preliminary assessment with Ricoh Theta S camera: 3D reconstruction with the (a) equidistant, (b) equisolid-angle, (c) stereographic and (d) orthogonal models
Figure 11 – Experiment A: (a) a top view and (b) a front view of 360° calibration field, illustrating the local reference system (orange) and the camera position (blue) where the fisheye images were taken; and (c) presents some Ricoh Theta video frames from sensor 1 taken in the 360° calibration field.
Figure 12 – Experiment B: (a) a top view of 360° calibration field, in which the local reference system (orange) and the Ricoh Theta sensor position and orientation (Sensor 1 – blue, Sensor 2 - red) were illustrated, (b) a sample of dual-fisheye images from Ricoh Theta sensor 1 (S1) and sensor 2 (S2).
Figure 13 – RMSE of discrepancies between control and estimated distance with the equidistant. equisolid-angle, stereographic and orthogonal models for both data sets48
Figure 14 - The estimated standard deviations of unit weight $(\sigma 0)$ for equisolid-angle and stereographic models with hemispheric and hyper-hemispheric point data set
Figure 15 – Average values of estimated standard deviation for (a) camera orientation angles: omega (σ_{ω}) , phi (σ_{ϕ}) and kappa (σ_{κ}) ; and (b) camera position $(\sigma_{X0}, \sigma_{Y0}, \sigma_{Z0})$ for equisolid- angle and stereographic models considering hemispheric (<i>hem</i>) and hyper-hemispheric (<i>hyp</i>) data sets.

Figure 16 – Correlation coefficient between principal distance c and (a) camera orientation (ω , φ , κ), and (b) camera perspective centre (X_0 , Y_0 , Z_0)
Figure 17 - Correlation coefficient between x-coordinate of principal point (x_0) and (a) camera orientation (ω, ϕ, κ) and (b) camera perspective centre (X_0, Y_0, Z_0) 53
Figure 18 - Correlation coefficient between y-coordinate of principal point (y_0) and (a) camera orientation $(\omega, \varphi, \kappa)$ and (b) camera perspective centre (X_0, Y_0, Z_0) 53
Figure 19 – The fisheye images used in the analysis of the coefficient correlation between IOPs $(c, x0, y0)$ and EOPs $(\omega, \phi, \kappa, X0, Y0, Z0)$
Figure 20 – (a) structure of the portable mobile terrestrial system (PMTS), (b) example of an operator carrying the PMTS, (c) Ricoh Theta omnidirectional system, and (c) components of the PMTS
Figure 21 – (a) Trajectory in the test area and the control points, (b) examples of control points in different heights and (c) a control point measurement
Figure 22 – Distances measurements of (a) façade, (b) traffic sign, and (c) pillar, for relative accuracy assessment.
Figure 23 – Generated point cloud of (a) sensor 1 and (b) sensor 2, and both point clouds attached in different perspectives (c) and (d)
Figure 24 – (a) Frontal and lateral view of the GoPro Fusion dual-camera, (b) fisheye images from sensor 1 (S1) and sensor 2 (S2) of the 360° camera calibration field, and (c) panoramic image obtained from GoPro desktop software.
Figure 25 – Fisheye images from each GoPro sensors of the 360° calibration field, pointing out the CTs that was used as constraints in the self-calibration.
Figure 26 – Fisheye image sequence of the citrus orchard taken with GoPro dual-camera70
Figure 27 - 3D reconstruction of the orange orchard: (a) top view of dense point cloud and cross section in green lines, and (b) longitudinal and transversal cross sections
Figure 28 - Examples of (a) a tree height measurement in the point cloud and (b) the 3D reconstruction of an orange fruit, the diameter measurement and the fitted sphere in CloudCompare
Figure 29 - Simulated data for preliminary experiments
Figure 30 – Projections of object points following the (a) equidistant, (b) equisolid-angle, (c) stereographic and (d) orthogonal models

LIST OF TABLES

Table 1 – Mathematical models for fisheye lens camera
Table 2 - Technical information of Ricoh Theta S camera
Table 3 – Sequence of calculations to determine 3D coordinates of points measured in circular target image
Table 4 – Parameters of Ricoh Theta S camera used in the preliminary study. These parameters were obtained from a camera calibration experiment based on equidistant model, performed by Campos et al. (2018a)
Table 5 - Effects of the distortions in the corner of the sensor for each fisheye model44
Table 6 - Mean, standard deviation and RMSE (in pixel) of image coordinates' residuals in the resultant component, and estimated standard deviation of unit weight (σ 0) for each fisheye model, in which <i>hem</i> is for hemispheric and <i>hyp</i> for hyper-hemispheric point data set45
Table 7 – Estimated values and standard deviations of IOPs for the equidistant, equisolid-angle, stereographic and orthogonal models using hemispheric data set
Table 8 – Estimated values and standard deviations of IOPs with the equisolid-angle, stereographic and orthogonal models for hyper-hemispheric data set and discrepancies of principal distance (c) and principal point coordinates (x_0, y_0) between equisolid-angle model and the others.
Table 9 - The average values of estimated standard deviations of EOPs for equidistant, equisolid-angle, stereographic and orthogonal using hemispheric data set
Table 10 - The average values of estimated standard deviations of EOPs for equisolid-angle, stereographic and orthogonal with hyper-hemispheric data set
Table 11 – The estimated IOPs and standard deviations in the simultaneous camera calibration of sensor 1 and sensor 2 of Ricoh Theta S camera for equisolid-angle and stereographic models with hemispheric data set.
Table 12 - The estimated IOPs and estimated standard deviations in the simultaneous camera calibration of sensor 1 and sensor 2 of Ricoh Theta S camera for equisolid-angle and stereographic models with hyper-hemispheric data set
Table 13 –ROPs and standard deviations of Ricoh Theta S camera for equisolid-angle and stereographic model with hemispheric (<i>hem</i>) and hyper-hemispheric (<i>hyp</i>) points data sets55
Table 14 - RMSE of discrepancies between control and estimated distances55
Table 15 – Average values and standard deviation of the components of relative rotation matrix, calculated for equisolid-angle and stereographic models with hyper-hemispheric point data set.
Table 16 – The discrepancies values, and mean, standard deviation and RMSE of discrepancies between distances measured directly in the test area and measured in the generated point cloud.

Γable 17 - Technical information of GoPro Fusion. 6	58
Table 18 - Estimated values of IOPs and the standard deviations for GoPro Fusion system7	71
Table 19 – Average values of ROPs components ($\Delta \omega$, $\Delta \varphi$ and $\Delta \kappa$ in degree and B_X , B_Y and B_Y and B_Y continueter) computed from the EOPs	
Table 20 - Tree heights measured in the generated dense point cloud	74
Γable 21 - Orange diameters manually measured in the generated point cloud and diameter obtained from the fitted spheres. 7	

SUMMARY

CHAPTER I INTRODUCTION

1 OVERVIEW AND MOTIVATION	15
1.1 OBJECTIVES	17
1.2 CONTENT	18
CHAPTER II	
LITERATURE REVIEW AND RELATED WORKS	
2 OPTICAL OMNIDIRECTIONAL SYSTEMS	19
2.1 MATHEMATICAL MODELS FOR PERSPECTIVE CAMERAS	20
2.2 MATHEMATICAL MODEL FOR FISHEYE LENSES	22
2.2 CAMERA CALIBRATION OF MULTI-CAMERA SYSTEM	28
CHAPTER III MATERIALS AND METHODS	
3. 360° CAMERA CALIBRATION FIELD	31
3.1 DUAL-FISHEYE CAMERA WITH HYPER-HEMISPHERICAL LENSES	32
3.1.1 Preliminary study with the Ricoh Theta S dual-camera	34
3.2 METHOD	
CHAPTER IV CALIBRATION ASSESSMENT OF A DUAL HEAD CAMERA - RICOH THE	ETA S
4 DATA SET	40
4.1 EXPERIMENTAL ASSESSMENT	40
4.1.2 Experiment A – Hyper-hemispherical lens camera calibration	40
4.1.2 Experiment B – Calibration of a dual-fisheye camera with hyper-hemispherical le	enses 42
4.2 RESULTS AND DISCUSSIONS	43
4.2.1 Experiment A - Assessment of fisheye models for hyper-hemispherical lenses	43
4.2.3 Exeperiment B - Dual-fisheye camera calibration	49
4.2.4 Experiment B – Assessment of the relative orientation	56
4.4 FINAL REMARKS	57

CHAPTER V

FESIABILITY STUDIES OF USING OMNIDIRECTIONAL SYSTEM FOR CLOSE-RANGE APPLICATIONS

5 OVERVIEW	59
5.1 ASSESSMENT OF A LOW-COST TERRESTRIAL MOBIL CITY MAPPING APPLICATIONS	
5.1.1 Portable mobile terrestrial system - PMTS	60
5.1.2 Experimental assessment	62
5.1.2.1 Data set	62
5.1.2.2 Photogrammetric process setup	63
5.1.2.3 Quality control	64
5.1.3 Results	65
5.2 3D RECONSTRUCTION OF CITRUS TREES USING OPTICAL SYSTEM	
5.2.1 Methodology	67
5.2.1.1 Camera calibration of GoPro 360 dual-camera	67
5.2.1.3 3D photogrammetric modelling	69
5.2.2 Results	71
5.2.2.1 Interior orientation parameters estimation	71
5.2.2.2 3D crop reconstruction	72
5.3 FINAL REMARKS	74
CHAPTER VI CONCLUSION AND RECOMENDAT	IONS
6 CONCLUSION	75
REFERENCES	77
APPENDIX A	84

CHAPTER I INTRODUCTION

1 OVERVIEW AND MOTIVATION

The design of high performance imaging systems to cover a full-spherical field of view (FOV) is a trend in the applied optical research. Multiple cameras arranged in the same structure, which enables a 360° FOV panorama, have been used for virtual reality, surveillance, robotic navigation and driverless vehicle applications. The overlap between images from each camera that composes the multi-camera system is an important issue to create panoramic images without blind zones. This is a current topic in recent works for multi-camera design (Fangi et al., 2013; Pernechele et al., 2018, Song et al., 2018, Ye et al., 2018, Lian et al., 2018). Furthermore, common points between sensor images can improve the system calibration, since the bundles of rays that formed the 360° image are considered.

A multi-camera system can be designed with perspectives lenses, which have a limited FOV, consequently, many cameras are needed to cover a full-spherical panorama. An example of omnidirectional system with perspectives cameras is Ladybug 5, which is composed of six cameras with 89.3° FOV (Khoramshahi et al., 2019). Another design option is to use fisheye lenses, in which fewer lenses are required to cover a large panorama due to the large FOV. The disadvantage is the loss of resolution caused by projection compression, mainly in the limits of the image. However, some authors have highlighted the benefits of using lenses with large FOV like fisheye lenses (Zhang et al., 2016; and Matsuki et al., 2018). For instance, a larger spatial distribution of points and a bigger overlap between sequence images can be tracked by fisheye lens cameras due to the large FOV.

Fisheye lenses can be classified as hemispherical (110° - 180° FOV) or hyperhemispherical (FOV above 180°). Nowadays, the use of lenses with FOV wider than 180° has been a trend in omnidirectional systems. Just two hyper-hemispherical lenses in back-to-back position can provide lightweight and low-cost full-spherical systems (e.g., Ricoh Theta S), while maintaining the overlap between sensor images. This compact design has motivated the use of dual-fisheye system in personal mobile terrestrial system for 360° imaging, as presented by Campos et al. (2018b). Furthermore, the complexity of camera calibration is reduced for dual-fisheye system, since only two sets of IOPs (interior orientation parameters) and EOPs (exterior orientation parameters) have to be

estimated. Reducing the number of camera to be triggered simultaneously also facilitate their synchronization.

Considering the high potential of 360° imaging for photogrammetric measurements (Campos et al., 2018b; Castanheiro et al., 2018; Castanheiro et al., 2020), some studies have focused on camera calibration (Aghayari et al., 2017; Campos et al., 2018a) and photogrammetric applications (Caruso et al., 2015; Meegoda et al., 2018; Perfetti et al., 2018; Campos et al., 2019; Tommaselli et al., 2019) of these multi-camera systems based on fisheye lenses. However, only few studies proposed mathematical models that consider the image observation geometry over 180° FOV for photogrammetric applications. Thus, these points are usually excluded from the photogrammetric procedure, such as camera calibration and image orientation. For instance, Campos et al. (2018a) presented a methodology to calibrate a multicamera system composed of two hyper-hemispherical fisheye cameras based on the equidistant mathematical model. In this work, the points in the hyper-hemispherical image field were removed from the camera calibration procedure because of the double mapping problem, which occurs due to the arctan function in the equidistant model. This problem was circumvented by Van den Heuvel et al. (2006) and Song et al. (2018) using a generic polynomial model to calibrate a hyper-hemispherical fisheye lens. Other models have been proposed in literature for hyper-hemispherical lens modelling (Khomutenko et al., 2016; Pernechele, 2016). However, fisheye projections models were not yet sufficiently explored for photogrammetric procedures with hyper-hemispherical lenses in the literature.

Besides a suitable mathematical model, an accurate multi-camera system calibration also depends on a suitable technique to estimate IOPs, EOPs and ROPs. Many researches have proposed a bundle adjustment with constraints on relative image orientation (He et al., 1993; Lerma et al., 2010; Habib et al., 2014; Detchev et al., 2018). Some studies have presented improvements in the multi-camera system calibration when using ROPs as stability constraints (Tommaselli et al., 2013; Lichti et al., 2015; Campos et al., 2018a; Jarron et al., 2019). This technique is based on the stability of the cameras during image acquisition. Nowadays, multi-camera systems have been constructed with cameras in a same structure, known as polydioptric system (Maas, 2008). This arrangement can design a more stable omnidirectional system. Therefore, the concept of stability constraints can be used as proposed by Tommaselli et al. (2009; 2013). Meanwhile, the use of relative orientation stability constraints, for dual-fisheye system, has been rarely approached in the literature.

This research presents a study on fisheye mathematical models based on equidistant, equisolid-angle, stereographic, and orthogonal projections combined with the Conrady-Brown distortion model. These models were tested in a camera calibration by bundle adjustment with the Ricoh Theta system to evaluate the contribution of using points in the hyper-hemispherical image field. The four fisheye models were assessed for the Ricoh Theta sensor using images taken in the 360° calibration field and CMC (calibration of multiple camera) software. The models that achieved the best results were implemented in the CMC software to calibrate both Ricoh Theta sensors in a simultaneous bundle adjustment based on stability constraints of relative rotation matrix and base element. A further analysis was performed for ROP estimation with and without using stability constraints. In this research, two experimental assessments with two different dual-fisheye systems in close-range applications were also performed: 3D city mapping using a PMTS (portable mobile terrestrial system), composed of Ricoh Theta S dual-camera; and 3D crop modelling using GoPro Fusion dualcamera. Both experimental assessments presented the potential of using an omnidirectional system to generate 3D point clouds, in which important attributes can be extracted depending on the application.

CHAPTER VI CONCLUSION AND RECOMENDATIONS

6 CONCLUSION

A mobile system with a dual-fisheye camera can be a feasible option. A larger spatial distribution of points can be obtained using a camera with larger FOV, mainly for environments with sparse features, such as indoor environments (Caruso et al., 2015; Matsuki et al., 2018). Another advantage is the larger overlap between sequential images; therefore, an object point is observed in a long period of image acquisition (Matsuki et al., 2018). The benefits on using large FOV images were presented in details by Zhang et al. (2016) and Matsuki et a. (2018). In this regards, fisheye models have been implemented in scientific and commercial software due to the growing use of fisheye images for accurate applications, which can be considered a trend in close range photogrammetry. However, some limitations when using a dual-fisheye camera can be highlighted.

Generally, dual-fisheye systems are composed of two hyper-hemispherical fisheye lenses to maintain the overlap between sensor images. Most of fisheye lenses follow the equidistant projection (Abraham and Frostner, 2005), as the Agisoft Photoscan/Metashape that uses the equidistant fisheye model. However, the equidistant model, as well orthogonal model, do not correctly model observations beyond 180°, being required to remove them to achieve accurate results (Campos et al., 2018a; Castanheiro et al., 2020). These common points between images from both sensors can improve some photogrammetric techniques, such as camera calibration. Therefore, further fisheye models were assessed with camera calibration bundle adjustment of one Ricoh Theta sensor. The equisolid-angle and stereographic models presented the best results. The a-posteriori values were 0.34 and 0.63 respectively, with a unit a-priori value, and both models achieved a RMSE of discrepancies between control and estimated distance of 6 mm. The affinity parameters were removed from the calibration procedures, since the effects in the image coordinates were less than 0.5 pixels.

Regarding the calibration of both Ricoh Theta sensors in the same process (simultaneous calibration with bundle adjustment), improvements were noticed in the estimated standard deviations of EOPs and IOPs when using points in the hyper-hemispherical image field, which were covered by both sensors. Furthermore, the use of ROPs as stability constraints improved the ROPs estimation. The best results for the calibration Ricoh Theta S dual-camera

were achieved by equisolid-angle model combined with Conrady-Brown's distortion model, considering the relative rotation elements and base components as stability constraints.

Two different dual-fisheye cameras (Ricoh Theta S and GoPro Fusion) were assessed for 3D modelling an urban area and an agricultural crop. Both experimental assessments presented that omnidirectional system composed of dual-fisheye camera can be a feasibility choice for 3D mapping. Considering the uncertainties in the process of generating 360° equirectangular images from Ricoh Theta S, the video frames are more suitable for applications that require high accuracy, such as close-range photogrammetry, because the original geometry is preserved. A disadvantage of fisheye video frames is the low resolution of the frames compared to the still image. Other omnidirectional system can be considered suitable to use in a portable mobile mapping, for instance, GoPro Fusion preserves the original fisheye images from each sensor without any processing, which is suitable for a rigorous photogrammetric chain.

Some recommendations for future works can be mentioned: (1) the calibration approach tested with Ricoh theta S system can be extended to other dual-fisheye systems, such as GoPro Fusion camera; (2) a comparative analysis with other fisheye models proposed in the literature and other techniques for multi-camera calibration can be also performed; (3) a stochastic weighting of observation can be insert, since the fisheye images have non-uniform spatial resolution; (4) the equisolid-angle projection model can be used for 3D reconstruction using hyper-hemispherical observations; and (5) a full-mapping can be achieved combining multi-sensor data, such as aerial images, LiDAR data and multispectral and hyperspectral images. These are investigations that may contribute to further studies on hyper-hemispherical fisheye models, improving the quality of results in applications.

REFERENCES

Abbas, A.; Douady-Pleven, C.; Macmillan, T. **Apparatus and methods for the storage of overlapping regions of imaging data for the generation of optimized stitched images**. U.S. Patent n. 10,194,097, 29 jan. 2019.

Abraham, S.; Förstner, W. Fish-eye-stereo calibration and epipolar rectification. **ISPRS Journal of photogrammetry and remote sensing**, v. 59, n. 5, p. 278-288, 2005.

Aghayari, S.; Saadatseresht, M.; Omidalizarandi, M.; Neumann, I. Geometric calibration of full spherical panoramic Ricoh-Theta camera. In: **ISPRS Annals of the Photogrammetry, Remote Sensing and Spatial Information Sciences**, v. 4, p. 237, 2017.

Agisoft, L. L. C. **Agisoft Metashape user manual**, Professional edition, Version 1.5. Agisoft LLC, St. Petersburg, Russia, from https://www.agisoft.com/pdf/metashape-pro_1_5_en.pdf. (2 July 2019).

An, G. H.; Lee, S.; Seo, M. W.; Yun, K.; Cheong, W. S.; Kang, S. J. Charuco board-based omnidirectional camera calibration method. **Electronics**, v. 7, n. 12, p. 421, 2018.

Baker, S.; Nayar, S. K. A theory of single-viewpoint catadioptric image formation. **International Journal of Computer Vision**, v. 35, n. 2, p. 175-196, 1999.

Barazzetti, L.; Previtali, M.; Roncoroni, F. Can we use low-cost 360 degree cameras to create accurate 3D models?. **International Archives of the Photogrammetry, Remote Sensing & Spatial Information Sciences**, v. 42, n. 2, 2018.

Barone, S.; Neri, P.; Paoli, A.; Razionale, A. V. Catadioptric stereo-vision system using a spherical mirror. **Procedia Structural Integrity**, v. 8, p. 83-91, 2018.

Basu, A.; Licardie, S. Alternative models for fish-eye lenses. **Pattern recognition letters**, v. 16, n. 4, p. 433-441, 1995.

Bazan, Wimerson Sanches. **Calibração de um Sistema dual de câmaras digitais.** 2008. Dissertação (Mestrado em Ciências Cartográficas) — Faculdade de Ciências e Tecnologia, Universidade Estadual Paulista, Presidente Prudente, 2008.

Bazan, W. S.; Tommaselli, A. M. G.; Galo, M.; Ruy, R. D. S. A Influência das Injunções de Orientação Relativa na Calibração de um Sistema Dual de Câmaras Digitais. **Boletim de Ciências Geodésicas**, v. 15, n. 3, p. 444-466, 2009.

Berveglieri, A.; Tommaselli, A.; Liang, X.; Honkavaara, E. Photogrammetric measurement of tree stems from vertical fisheye images. **Scandinavian journal of forest research**, v. 32, n. 8, p. 737-747, 2017.

Brown, D. C. Close-range camera calibration. **Photogrammetric Engineering**, v. 37, n.8, p. 855-866, 1971.

- Calantropio, A.; Chiabrando, F.; Einaudi, D.; Teppati Losè, L. 360° images for uav multisensor data fusion: first tests and results. **International Archives of the Photogrammetry, Remote Sensing & Spatial Information Sciences**, v.42, n 13. 2019.
- Campos, M.; Tommaselli, A.; Ivánová, I.; Billen, R. Data product specification proposal for architectural heritage documentation with photogrammetric techniques: a case study in Brazil. **Remote Sensing**, v. 7, n. 10, p. 13337-13363, 2015.
- Campos, M. B.; Tommaselli, A. M. G.; Marcato Junior, J.; Honkavaara, E. Geometric model and assessment of a dual-fisheye imaging system. **The Photogrammetric Record**, 2018a.
- Campos, M. B.; Tommaselli, A. M. G.; Honkavaara, E.; Prol, F. D. S.; Kaartinen, H.; El Issaoui, A.; Hakala, T. A Backpack-Mounted Omnidirectional Camera with Off-the-Shelf Navigation Sensors for Mobile Terrestrial Mapping: Development and Forest Application. **Sensors**, v. 18, n. 3, p. 827, 2018b.
- Campos, M. B.; Tommaselli, A. M. G.; Castanheiro, L. F.; Oliveira, R. A.; Honkavaara, E. A Fisheye Image Matching Method Boosted by Recursive Search Space for Close Range Photogrammetry. **Remote Sensing**, v. 11, n. 12, p. 1404, 2019.
- Caruso, D.; Engel, J.; Cremers, D. Large-scale direct SLAM for omnidirectional cameras. In: 2015 IEEE/RSJ International Conference on Intelligent Robots and Systems (IROS). **Proceedings[...]**, IEEE, 2015. p. 141-148. 2015.
- Castanheiro, L. F.; Campos, M. B.; Tommaselli, A. M. G. Análise da viabilidade de um sistema de mapeamento móvel terrestre de baixo custo para cadastro territorial urbano. In: XIII Congresso Brasileiro de Cadastro Técnico Multifinalitário e Gestão Territorial (COBRAC), 2018. **Proceedings[...].** Florianópolis: UFSC, 2018.
- Castanheiro, L. F.; Tommaselli, A. M. G.; Campos, M. B.; Berveglieri, A.; Santos, G. 3D reconstruction of citrus trees using an omnidirectional optical system. In LAGIRS 2020: 2020 Latin American GRSS & ISPRS Remote Sensing Conference. **To be published**, 2020.
- Conrady, A. Decentered lens systems. **Monthly Notices of the Royal Astronomical Society**, 79(5): 384–390, 1919.
- Courbon, J.; Mezouar, Y.; Eckt, L.; Martinet, P. A generic fisheye camera model for robotic applications. In: 2007 IEEE/RSJ International Conference on Intelligent Robots and Systems. **Proceedings**[...], IEEE, p. 1683-1688, 2007.
- Deng, L., Mao, Z., Li, X., Hu, Z., Duan, F., Yan, Y. UAV-based multispectral remote sensing for precision agriculture: A comparison between different cameras. **ISPRS journal of photogrammetry and remote sensing**, 146, 124-136. 2018
- Detchev, I.; Habib, A.; Mazaheri, M.; Lichti, D. Practical in situ implementation of a multicamera multisystem calibration. **Journal of Sensors**, v. 2018, p. 12, 2018.
- Devernay, F.; Faugeras, O. Straight lines have to be straight. **Machine vision and applications**, v. 13, n. 1, p. 14-24, 2001.

- Ericson, S.; Åstrand, B. Row-detection on an agricultural field using omnidirectional camera. In 2010 IEEE/RSJ International Conference on Intelligent Robots and Systems, **Proceedings[...].** Taipei, Taiwan, 4982-4987. 2010.
- Escolà, A.; Martinez-Casasnovas, J. A.; Rufat, J; Arno, J.; Arbone´S, A.; Sebe, F.; Pascual, M.; Gregorio, E.; Rosell-Polo, J. R. Mobile terrestrial laser scanner applications in precision fruticulture/horticulture and tools to extract information from canopy point clouds. **Precision Agriculture**, v. 18, n. 1, p. 111-132, 2017.
- Fangi, G.; Nardinocchi, C. Photogrammetric processing of spherical panoramas. **The photogrammetric record**, v. 28, n. 143, p. 293-311, 2013.
- Fraser, C. S. Digital camera self-calibration. **ISPRS Journal of Photogrammetry and Remote sensing**, v. 52, n. 4, p. 149-159, 1997.
- Galo, M.; Tommaselli, A. M. G.; Hasegawa, J. K.; Camargo, P. D. O. Significância dos parâmetros de orientação interior na calibração de câmaras. In: II SIMGEO-Simpósio Brasileiro de Ciências Geodésicas e Tecnologias da Geoinformação, **Proceedings[...].** Recife, Brazil, p. 1-9, 2008.
- Galo, M.; Tommaselli, A. M. G.; Hasegawa, J. K.; Ruy, R., Reis, T. Mudança da temperatura e efeitos na calibração de câmaras digitais: estudo de caso. In: III Simpósio Brasileiro de Ciências Geodésicas e Tecnologias da Geoinformação, **Proceedings**[...]. Recife, Brazil, 2010.
- Habib, A.; Morgan, M. Stability analysis and geometric calibration of off-the-shelf digital cameras. **Photogrammetric Engineering & Remote Sensing**, v. 71, n. 6, p. 733-741, 2005.
- Habib, A.; Jarvis, A.; Detchev, G.; Stensaas, D.; Moe, D.; Christopherson, J. Standards and specifications for the calibration and stability of amateur digital cameras for close-range mapping applications. **International Archives of Photogrammetry, Remote Sensing and Spatial Information Sciences**, v. 37, 2008.
- Habib, A.; Detchev, I.; Kwak, E. Stability analysis for a multi-camera photogrammetric system. **Sensors**, v. 14, n. 8, p. 15084-15112, 2014.
- He, G.; Novak, K.; Feng, W. Stereo camera system calibration with relative orientation constraints. In: Videometrics. **Proceedings[...].** International Society for Optics and Photonics, 1993. p. 2-8. 1993.
- Hughes, C.; Denny, P.; Jones, E.; Glavin, M. Accuracy of fish-eye lens models. **Applied Optics**, v. 49, n. 17, p. 3338–3347, 2010.
- INTERNATIONAL ORGANIZATION FOR STANDARDIZATION. **ISO 19157**: Geographic information- Quality principles. Suíça, 2002.
- Jarron, D.; Lichti, D. D.; Shahbazi, M. M.; Radovanovic, R. S. Multi-camera panormamic imaging system calibration. In: 11th International Conference on Mobile Mapping. **Proceedings[...]**. Shenzhen, China, 2019.

- Ji, S.; Qin, Z.; Shan, J.; Lu, M. Panoramic SLAM from a multiple fisheye camera rig. **ISPRS Journal of Photogrammetry and Remote Sensing**, v. 159, p. 169-183, 2020.
- Kannala, J.; Brandt, S. S. A generic camera model and calibration method for conventional, wide-angle, and fish-eye lenses. **IEEE transactions on pattern analysis and machine intelligence**, v. 28, n. 8, p. 1335-1340, 2006.
- Khomutenko, B.; Garcia, G.; Martinet, P. An enhanced unified camera model. **IEEE Robotics** and Automation Letters, v. 1, n. 1, p. 137-144, 2015.
- Khoramshahi, E.; Honkavaara, E. Modelling and automated calibration of a general multiprojective camera. **The Photogrammetric Record**, v. 33, n. 161, p. 86-112, 2018.
- Khoramshahi, E.; Campos, M. B.; Tommaselli, A. M. G.; Vilijanen, N.; Mielonen, T.; Kaartinen, H.; Kukko, A.; Honkavaara, E. Accurate calibration scheme for a multi-camera mobile mapping system. **Remote Sensing**, v. 11, n. 23, p. 2778, 2019.
- Lehtola, V. V.; Kaartinen, H.; Nüchter, A.; Kaijaluoto, R.; Kukko, A.; Litkey, P.; Kurkela, M. Comparison of the selected state-of-the-art 3D indoor scanning and point cloud generation methods. **Remote Sensing**, v. 9, n. 8, p. 796, 2017.
- Lerma, J. L.; Navarro, S.; Cabrelles, M.; Seguí, A. E. Camera calibration with baseline distance constraints. **The Photogrammetric Record**, 25(130), 140-158, 2010.
- Lichti, D. D.; Sharma, G. B.; Kuntze, G.; Mund, B.; Beveridge, J. E.; Ronsky, J. L. Rigorous geometric self-calibrating bundle adjustment for a dual fluoroscopic imaging system. **IEEE transactions on medical imaging**, v. 34, n. 2, p. 589-598, 2015.
- Loch, C.; Erba, D. A. Cadastro técnico multifinalitário rural e urbano. Cambridge, MA: Lincoln Institute of Land Policy, 146p. 2007
- Luhmann, T.; Fraser, C.; Maas, H. G. Sensor modelling and camera calibration for close-range photogrammetry. **ISPRS Journal of Photogrammetry and Remote Sensing**, v. 115, p. 37-46, 2016
- Maas, H. Close-range photogrammetry sensors. In: Li, Z., Chen, J., Balsavias, E., **Advances in Photogrammetry, Remote Sensing and Spatial Information Science:** 2008 ISPRS Congress Book. New York, USA, pp. 63-72. 2008.
- Marcato Junior, J.; Moraes, M. V. A.; Tommaselli, A. M. G. Experimental assessment of techniques for fisheye camera calibration. **Boletim de Ciências Geodésicas**, v.21, n.3, p. 637-651, 2015.
- Marcato Junior, J.; Tommaselli, A. M. G.; Moraes, M. V. A. Calibration of a catadioptric omnidirectional vision system with conic mirror. **ISPRS Journal of Photogrammetry and Remote Sensing**, v. 113, p. 97-105, 2016.
- Matsuki, H.; von Stumberg, L.; Usenko, V.; Stückler, J.; Cremers, D. Omnidirectional DSO: Direct sparse odometry with fisheye cameras. **IEEE Robotics and Automation Letters**, v. 3, n. 4, p. 3693-3700, 2018.

Meegoda, J. N.; Kewalramani, J. A.; Saravanan, A. Adapting 360-Degree Cameras for Culvert Inspection: Case Study. **Journal of Pipeline Systems Engineering and Practice**, v. 10, n. 1, p. 05018005, 2019.

Mei, C.; Benhimane, S.; Malis, E.; Rives, P. Constrained Multiple Planar Template Tracking for Central Catadioptric Cameras. In: BMVC. **Proceedings[...]**, p. 619-628. 2006.

Mei, C.; Rives, P. Single view point omnidirectional camera calibration from planar grids. In: Proceedings 2007 IEEE International Conference on Robotics and Automation. **Proceedings[...]** Roma, Italy: IEEE, 2007. p. 3945-3950, 2007.

Mikhail, E. M.; Ackerman, F. **Observations and Least Squares**, 1st ed; IEP, New York NY, USA, 1976, 497p.

Mikhail, E. M.; Bethel, J. S.; Mcglone, J. C. **Introduction to modern photogrammetry.** New York, 2001.

Moniwa, H. The concept of "photo-variant" self-calibration and its application in block adjustment with bundles. **Photogrammetria**, v. 36, n. 1, p. 11-29, 1981.

Moriya, É. A. S., Imai, N. N., Tommaselli, A. M. G., Berveglieri, A., Honkavaara, E., Soares, M. A., Marino, M.. Detecting citrus huanglongbing in brazilian orchards using hyperspectral aerial images. **International Archives of the Photogrammetry, Remote Sensing and Spatial Information Sciences**, XLII-2/W13, 1881-1886. 2019.

Pajdla, T.; Bakstein, H. Panoramic mosaicing with a 180 field of view lens. In: IEEE Workshop on Omnidirectional Vision. **Proceedings**[...], Copenhagen, Denmark, 2002. p. 60-67. 2002.

Perfetti, L.; Polari, C.; Fassi, F. Fisheye multi-camera system calibration for surveying narrow and complex architectures. **The International Archives of the Photogrammetry, Remote Sensing and Spatial Information Sciences**, v. 42, n. 2, p. 877-883, 2018.

Pernechele, C. Hyper hemispheric lens. **Optics express**, v. 24, n. 5, p. 5014-5019, 2016.

Pernechele, C.; Dionisio, C.; Munari, M.; Opromolla, R.; Rufino, G.; Fasano, G.; Grassi, M.; Pastore, S. Hyper hemispheric lens applications in small and micro satellites. **Advances in Space Research**, v. 62, n. 12, p. 3449-3461, 2018.

Pessoa, G. G.; Santos, R. C.; Carrilho, A. C.; Galo, M.; Amorim, A. Urban scene classification using features extracted from photogrammetric point clouds acquired by uav. **International Archives of the Photogrammetry, Remote Sensing & Spatial Information Sciences**, v.42, n.2, p. 511-518, 2019.

Prosdocimi, M., Burguet, M., Di Prima, S., Sofia, G., Terol, E., Comino, J. R., Cerdà, A. Tarolli, P. Rainfall simulation and Structure-from-Motion photogrammetry for the analysis of soil water erosion in Mediterranean vineyards. **Science of the Total Environment**, 574, 204-215. 2017

Ray, A. Applied Photographic Optics: Lenses and Optical Systems for Photography, Film, Video and Electronic Imaging. Oxford, UK, 2002.

Remondino, F.; Fraser, C. S. Digital camera calibration methods: considerations and comparisons. **The International Archives of Photogrammetry, Remote Sensing and Spatial Information Sciences**, v. 36, n. 5, p. 266-272, 2006.

Sahin, C. Comparison and calibration of mobile phone fisheye lens and regular fisheye lens via equidistant model. **Journal of Sensors**, v. 2016, 2016.

Scaramuzza, D; Martinelli, A.; Siegwart, R. A toolbox for easily calibrating omnidirectional cameras. In: 2006 IEEE/RSJ International Conference on Intelligent Robots and Systems. **Proceedings[...].** Beijing: IEEE, p. 5695-5701, 2006.

Schneider, D.; Schwalbe, E.; Maas, H. G. Validation of geometric models for fisheye lenses. **ISPRS Journal of Photogrammetry and Remote Sensing.** v. 64, n.3, p. 259-266, 2009.

Song, W.; Liu, X.; Lu, P.; Huang, Y.; Weng, D.; Zheng, Y.; Liu, Y.; Wang, Y. Design and assessment of a 360° panoramic and high-performance capture system with two tiled catadioptric imaging channels. **Applied optics**, v. 57, n. 13, p. 3429-3437, 2018.

Sturm, P.; Ramalingam, S.; Tardif, J. P.; Gasparini, S.; Barreto, J. Camera models and fundamental concepts used in geometric computer vision. **Foundations and Trends® in Computer Graphics and Vision**, v. 6, n. 1–2, p. 1-183, 2011.

Sun, Z.; Zhang, Y. Accuracy evaluation of videogrammetry using a low-cost spherical camera for narrow architectural heritage: An observational study with variable baselines and blur filters. **Sensors**, v. 19, n. 3, p. 496, 2019.

Theta Developers. **Proprietary Technical Information: Lens Parameter Information.** Disponível em: < http://theta360.guide/community-document/community.html> Accessed on 19 April 2017.

Tommaselli, A. M. G.; Tozzi, C. L. Técnicas de calibração de câmaras em visão computacional. **Jornada EPUSP/IEEE em Computação Visual**, Dezembro, 1990.

Tommaselli, A. M. G.; Tozzi, C. L. A recursive approach to space resection using straight lines. **Photogrammetric Engineering and Remote Sensing**, p. 57-66, 1996.

Tommaselli, A. M. G.; Galo, M.; Bazan, W. S.; Ruy, R. S.; Junior, J. M. Simultaneous calibration of multiple camera heads with fixed base constraint. In the 6th International Symposium on Mobile Mapping Technology. **Proceedings[...]** Presidente Prudente, São Paulo, Brazil, 2009.

Tommaselli, A. M. G.; Marcato Junior, J.; Telles, S. S. S. Camera calibration using straight lines: assessment of a model based on plane equivalence. **Photogrammetric Journal of Finland**, v. 23, n. 1, p. 1-11, 2012.

Tommaselli, A.; Galo, M.; Moraes, M.; Marcato Junior, J.; Caldeira, C.; Lopes, R. Generating virtual images from oblique frames. **Remote Sensing**, v. 5, n. 4, p. 1875-1893, 2013.

Tommaselli, A. M. G.; Marcato Junior, J.; Moraes, M. V. A.; Silva, S. L. A.; Artero, A. O. Calibration of panoramic cameras with coded targets and a 3D calibration field. **The International Archives of Photogrammetry, Remote Sensing and Spatial Information Sciences**, v. 40, n. 3, p. 137, 2014.

Tommaselli, A. M. G.; Galo, M.; Dos Reis, T. T.; Da Silva Ruy, R.; De Moraes, M. V. A.; Matricardi, W. V. Development and Assessment of a Data Set Containing Frame Images and Dense Airborne Laser Scanning Point Clouds. **IEEE Geoscience and Remote Sensing Letters**, v. 15, n. 2, p. 192-196, 2018.

Tommaselli, A. M.; Campos, M. B.; Castanheiro, L. F.; Honkavaara, E. A feasibility study on incremental bundle adjustment with fisheye images and low-cost sensors. **International Archives of Photogrammetry, Remote Sensing and Spatial Information Sciences**, v. 42, p. 167-171, 2019.

Usenko, V.; Demmel, N.; Cremers, D. The Double Sphere Camera Model. In: **2018** International Conference on 3D Vision (3DV). IEEE, p. 552-560, 2018.

Van Den Heuvel, F. A.; Verwaal, R.; Beers, B. Calibration of fisheye camera systems and the reduction of chromatic aberration. **International Archives of Photogrammetry, Remote Sensing and Spatial Information Sciences**, v. 36, n. 5, p. 6, 2006.

Wolfert, S., Ge, L., Verdouw, C., Bogaardt, M. J. Big data in smart farming—a review. **Agricultural Systems**, 153, 69-80. 2017.

Xue, Z.; Xue, N.; Xia, G. S.; Shen, W. Learning to calibrate straight lines for fisheye image rectification. **arXiv preprint arXiv:1904.09856**, 2019.

Ye, W. W.; Zeng, Z. H.; Lin, F. Design of compact panoramic lens. In: 9th International Symposium on Advanced Optical Manufacturing and Testing Technologies: Meta-Surface-Wave and Planar Optics, **Proceedings[...]**. International Society for Optics and Photonics, 2019. p. 1084114.

Zhang, Z. A flexible new technique for camera calibration. **IEEE Transactions on pattern analysis and machine intelligence**, v. 22, 2000.

Zhang, Z.; Rebecq, H.; Forster, C.; Scaramuzza, D. Benefit of large field-of-view cameras for visual odometry. In: 2016 IEEE International Conference on Robotics and Automation (ICRA). **Proceedings[...].** IEEE, 2016. p. 801-808.